



LAWRENCE  
LIVERMORE  
NATIONAL  
LABORATORY

# Quantum-Mechanical Interatomic Potentials with Electron Temperature for Strong Coupling Transition Metals

J. A. Moriarty, R. Q. Hood, L. H. Yang

June 14, 2011

Physical Review Letters

## **Disclaimer**

---

This document was prepared as an account of work sponsored by an agency of the United States government. Neither the United States government nor Lawrence Livermore National Security, LLC, nor any of their employees makes any warranty, expressed or implied, or assumes any legal liability or responsibility for the accuracy, completeness, or usefulness of any information, apparatus, product, or process disclosed, or represents that its use would not infringe privately owned rights. Reference herein to any specific commercial product, process, or service by trade name, trademark, manufacturer, or otherwise does not necessarily constitute or imply its endorsement, recommendation, or favoring by the United States government or Lawrence Livermore National Security, LLC. The views and opinions of authors expressed herein do not necessarily state or reflect those of the United States government or Lawrence Livermore National Security, LLC, and shall not be used for advertising or product endorsement purposes.

# Quantum-Mechanical Interatomic Potentials with Electron Temperature for Strong Coupling Transition Metals

John A. Moriarty,\* Randolph Q. Hood and Lin H. Yang

Condensed Matter and Materials Division

Lawrence Livermore National Laboratory

Livermore, CA 94551-0808

## Abstract

In narrow  $d$ -band transition metals, electron temperature  $T_{el}$  can impact the underlying electronic structure for temperatures near and above melt, strongly coupling the ion- and electron-thermal degrees of freedom and producing  $T_{el}$ -dependent interatomic forces. Starting from the Mermin formulation of density functional theory (DFT), we have extended first-principles generalized pseudopotential theory (GPT) to finite electron temperature, and then developed efficient  $T_{el}$ -dependent *model* GPT (MGPT) interatomic potentials for a Mo prototype. Unlike potentials based on the  $T_{el} = 0$  electronic structure, the  $T_{el}$ -dependent MGPT potentials yield a high-pressure Mo melt curve consistent with DFT quantum simulations as well as with dynamic experiments, and also support a rich polymorphism in the high- $T,P$  phase diagram.

PACS: 71.15.-m, 34.20.Cf, 64.70.D-, 81.30.Bx

\*Corresponding author, email: moriarty2@llnl.gov

In the past decade, high-pressure melting in  $d$ -band transition metals [1-11] and the possibility of a solid-phase polymorphism beneath the melt curve [6,9-11] have been subjects of widespread experimental [1-4] and theoretical [5-11] interest as well as considerable controversy. The present paper focuses on two important, but largely overlooked, theoretical aspects of this problem, namely, (i) the key role of *electron temperature*  $T_{\text{el}}$  in such materials near melt, especially for  $3d$  and  $4d$  metals; and (ii) the construction from density-functional-theory (DFT) quantum mechanics [12] of corresponding  $T_{\text{el}}$ -*dependent* interatomic potentials, which can provide up to six orders of magnitude increase in computational speed over DFT quantum simulations [5,7-9,11,13] and are needed for a wider investigation of structural, thermodynamic, defect and mechanical properties. As shown in Fig. 1 for bcc Mo, the effect of temperature on the DFT electronic structure near melt can be quite strong. Such narrow-band transition metals have large densities of electronic states, leading to strong coupling between ion- and electron-thermal degrees of freedom at high temperature. Consequently,  $T_{\text{el}}$  can affect the interatomic forces that control the phase diagram and melt.

The first indication of the possible importance of electron temperature in transition-metal melting occurred nearly two decades ago with the initial quantum-based calculation of the high-pressure melt curve in Mo [14]. This calculation was performed in the conventional *weak-coupling* thermodynamic limit, where the Helmholtz free energy  $A_{\text{tot}}$  at atomic volume  $\Omega$  and ion temperature  $T = T_{\text{ion}}$  is obtained as a sum of separate cold, ion-thermal and electron-thermal contributions based on the  $T_{\text{el}} = 0$  electronic structure:

$$A_{\text{tot}}(\Omega, T) = E_0(\Omega) + A_{\text{ion}}(\Omega, T) + A_{\text{el}}(\Omega, T). \quad (1)$$

In this model,  $A_{\text{el}} \propto \rho(E_{\text{F}})T^2$ , where  $\rho(E_{\text{F}})$  is the  $T_{\text{el}} = 0$  electronic density of states (DOS) at the Fermi level  $E_{\text{F}}$ . The striking result obtained in Ref. 14 was that, in the absence of  $A_{\text{el}}$ , calculated melt temperatures were found to be too large by a factor of two. Lowering the Mo zero-pressure melt point close its observed value thus required a very large increase in  $\rho(E_{\text{F}})$  going from the solid to the liquid, thereby demonstrating that  $A_{\text{el}}$  is not a small correction to  $A_{\text{ion}}$ , as is implicitly assumed in this model.

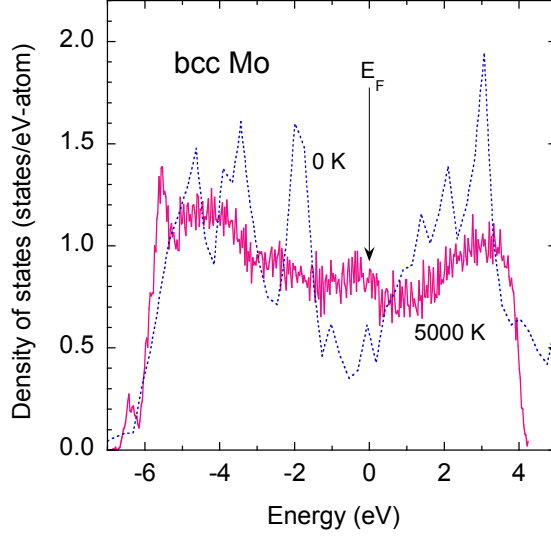


**Fig. 1** Strong dependence of the electronic density of states on temperature in bcc Mo, as obtained by the present DFT quantum simulations at an atomic volume of 92.99 a.u. Upper temperature of 5000 K represents conditions near melt for this volume.

While the weak-coupling model works well in wider  $5d$  metals such as Ta [6], where  $A_{el}$  is only a 5% correction in Eq. (1), this model fails in Mo due to the fact that  $T_{el}$  significantly alters the physics in this case. Because the DOS varies strongly with temperature in Mo (Fig. 1), its change upon melting is actually much less than calculated in the weak-coupling model. In addition, a high  $T_{el}$  softens interatomic forces and hence the shear elastic moduli and phonons, as illustrated in Fig. 2 for  $C'$  in bcc Mo. Here  $C'$  is lowered by 15 – 35% at melt due to  $T_{el}$  alone, with  $T_{ion} = 0$  in these calculations. As a result, energy barriers are lowered by  $T_{el}$  in the bcc solid, leading to lowered melt temperatures and the appearance of other competitive solid phases.

To go beyond the weak-coupling model and develop first-principles  $T_{el}$ -dependent interatomic potentials, our starting point is the finite-temperature Mermin formulation of DFT [12]. In particular, we focus on the grand potential  $Q_{el}$ , which replaces the total energy  $U_{tot}$  as the variational functional of electron density  $n_{el}(\vec{r})$  in the grand canonical ensemble (constant  $\Omega$ ,  $T_{el}$  and chemical potential  $\mu_{el}$ ):

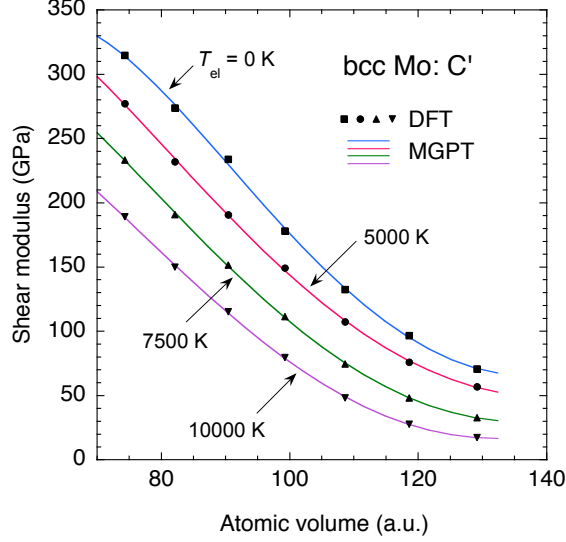


**Fig. 2** Dependence of the of the shear modulus  $C'$  on electron temperature  $T_{el}$  in Mo, as determined from first-principles DFT calculations performed in the static bcc lattice with  $T_{ion} = 0$ , and as used here to constrain  $T_{el}$ -dependent MGPT potentials.

$$\begin{aligned}
 Q_{el} &= U_{tot} - T_{el}S_{el} - \mu_{el}N_{el} \\
 &= -\int_0^{\infty} f_{FD}(E)N(E)dE + U_{rest}
 \end{aligned} \tag{2}$$

Here  $S_{el}$  is the electronic entropy,  $N_{el}$  the number of electrons,  $f_{FD}(E)$  the Fermi-Dirac occupation function  $(1 + \exp[(E - \mu_{el})/k_B T])^{-1}$ ,  $N(E)$  the integrated DOS,  $\int_0^E \rho(E')dE'$ , and  $U_{tot} = U_{band} + U_{rest}$ , where  $U_{band}$  is the band-structure energy and  $U_{rest}$  contains the remaining electrostatic, double-counting and exchange-correlation terms. The key point about the second line of Eq. (2) is that both  $N(E)$  and  $U_{rest}$  are functionals of  $n_{el}$  that can be developed rigorously in multi-ion expansions. These expansions have been obtained previously for transition metals within DFT at  $T_{el} = 0$  via first-principles generalized pseudopotential theory (GPT) [15], using a quantum-mechanical basis set of plane waves and localized, atomic-like  $d$  states. Extension of these results to finite electron temperature is accomplished by appropriate insertion of the Fermi-Dirac function  $f_{FD}(E)$  in the energy integrals establishing  $n_{el}$ . The multi-ion expansions for  $N(E)$  and  $U_{rest}$  obtained in Ref. 15 are then directly transferable to Eq. (2).

In molecular dynamics (MD) simulations, we work in the equivalent canonical ensemble (constant  $\Omega$ ,  $T_{\text{el}}$  and  $N_{\text{el}}$ ), where  $Q_{\text{el}}$  is replaced by the free energy  $F_{\text{el}} = U_{\text{tot}} - T_{\text{el}}S_{\text{el}}$ . Within the GPT, we have developed  $F_{\text{el}}$  as a functional of the  $N$  ion positions  $\vec{R} \equiv \{\vec{R}_i\}$  in terms of  $T_{\text{el}}$ -dependent multi-ion potentials up to four-ion interactions:

$$F_{\text{el}}(\vec{R}; \Omega, T_{\text{el}}) = NF_{\text{vol}}(\Omega, T_{\text{el}}) + \frac{1}{2} \sum_{i,j} v_2(ij; \Omega, T_{\text{el}}) + \frac{1}{6} \sum_{i,j,k} v_3(ijk; \Omega, T_{\text{el}}) + \frac{1}{24} \sum_{i,j,k,l} v_4(ijkl; \Omega, T_{\text{el}}) \quad (3)$$

Here the leading volume term  $F_{\text{vol}}$ , as well the interatomic potentials  $v_2$ ,  $v_3$  and  $v_4$ , are structure independent and transferable to all bulk ion configurations. These quantities are not analytic functions, but they are explicit functionals of the  $sp$  pseudopotential,  $d$ - $d$  tight-binding and  $sp$ - $d$  hybridization matrix elements arising in the chosen basis set. In a simulation, the force on each ion is calculated from the gradient of  $F_{\text{el}}$  with respect to its position. If the ions are equilibrated at temperature  $T = T_{\text{ion}}$ , then the Helmholtz free energy of the system is  $A_{\text{tot}}(\Omega, T) = \langle F_{\text{el}} \rangle - TS_{\text{ion}}$ , where the first term is a configuration average of  $F_{\text{el}}$  and  $S_{\text{ion}}$  is the ion entropy. This replaces Eq. (1). Note that because the electrons and ions are separately equilibrated, our formalism applies equally to all values of the electron temperature, including the limiting cases  $T_{\text{el}} = 0$ ,  $T_{\text{el}} = T_{\text{ion}}$  and  $T_{\text{el}} \gg T_{\text{ion}}$ . The latter occurs, for example, in ultra-fast femtosecond laser experiments in which the electrons are rapidly heated before the ions can move [16]. This is the extreme case where melt depends strongly on electron temperature, but as we show below such is already true in Mo at  $T_{\text{el}} = T_{\text{ion}}$ .

For large-scale MD simulations, the  $T_{\text{el}}$ -dependent GPT has two practical limitations: (i) the potentials are long-ranged due to the  $sp$ - $d$  hybridization contributions; and (ii)  $v_3$  and  $v_4$  are multi-dimensional functions that can't be tabulated and must be recalculated at each time step. To overcome these limitations, we have extended the simplified *model* GPT (MGPT) developed at  $T_{\text{el}} = 0$  [14,17] to finite electron temperature, introducing several systematic approximations to the  $T_{\text{el}}$ -dependent GPT appropriate for nearly half-

filled  $d$ -band metals like Mo. The main approximations are the neglect of explicit  $sp$ - $d$  hybridization contributions and the use of non-canonical  $d$  bands [17] to express the remaining  $d$ - $d$  tight-binding matrix elements analytically. The latter matrix elements then have a simple  $r^{-p}$  radial dependence and an angular dependence quantified by the ratios  $c_0 = dd\sigma / dd\delta$  and  $c_1 = dd\pi / dd\delta$ . Highly symmetric canonical  $d$  bands, which heretofore have been used in  $T_{el} = 0$  MGPT applications to Mo [14,17], are recovered in the limits  $p = 2\ell + 1 = 5$  (for  $\ell = 2$ ),  $c_0 = 6$  and  $c_1 = -4$ . In the  $T_{el}$ -dependent MGPT, the  $d$ -state contributions to  $v_2$ ,  $v_3$  and  $v_4$  are expressed as a series of five terms, each involving an  $\Omega$ - and  $T_{el}$ -dependent coefficient, a single radial function  $f(r) = (R_{ws} / r)^p$ , where  $R_{ws}$  is the Wigner-Seitz radius, and for  $v_3$  and  $v_4$ , three angular functions  $L$ ,  $P$  and  $M$ , which are defined in Ref. 17. The latter functions are evaluated on the fly at each time step in the simulation by  $d$ -state matrix multiplication. In the case of Mo, the five coefficients together with  $F_{vol}$  are established by fitting, as a function of  $\Omega$  and  $T_{el}$ , first-principles DFT data at  $T_{ion} = 0$  on the bcc equation of state, shear elastic moduli (Fig. 2), unrelaxed vacancy formation energy, and mean-squared phonon frequency.

The use of non-canonical  $d$  bands in the case of Mo is a highly significant improvement, especially in the MGPT description of the phonons. This is due to the well-known Kohn-like anomalies in the Mo phonon spectrum, which are not adequately captured by canonical  $d$  bands. In this regard, the remaining parameters  $p$ ,  $c_0$  and  $c_1$  have been determined in the following way. The parameter  $p$  was chosen to decrease slowly and smoothly with increasing  $\Omega$  and  $T_{el}$ , within the narrow physical range  $4.0 \leq p \leq 5.2$ . For each  $T_{el}$ , the parameters  $c_0$  and  $c_1$  were determined at a single volume (105.1 a.u.) by a least-squares fit to first-principles DFT values of the four high symmetry zone-boundary phonon frequencies at the H and N points in the Brillouin zone. Remarkably, the same values of  $c_0$  and  $c_1$  also optimize the calculated phonons at all volumes for a given  $T_{el}$ , such that all phonons at all volumes are improved with just two parameters, as illustrated in Fig. 3 for the anomalous H-point phonon. The result is DFT-accurate MGPT phonon spectra over the entire  $\Omega$  and  $T_{el}$  ranges considered.

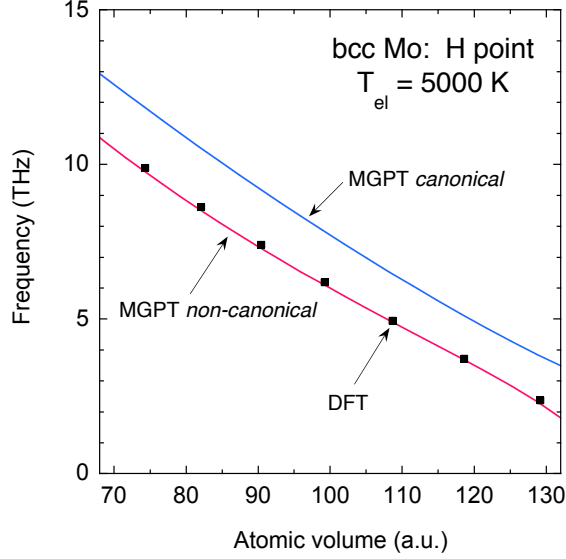


**Fig. 3** Large positive impact of non-canonical  $d$  bands on the  $T_{el}$ -dependent MGPT calculation of the anomalous H-point phonon frequency and its volume dependence in bcc Mo at an electron temperature of 5000 K.

The supporting first-principles DFT calculations used to constrain and validate the MGPT potentials were performed with an accurate plane-wave pseudopotential method [13]. For Mo, a nonlocal norm-conserving pseudopotential was constructed to treat the six  $5s$ ,  $5p$  and  $4d$  valence electrons over the atomic volume range  $70 \leq \Omega \leq 130$  a.u., with a non-local treatment for the  $p$  and  $d$  states and a local treatment for the  $s$  states. A plane-wave energy cutoff of 80 Ry was employed, except in the case of our quantum molecular dynamics (QMD) simulations of melt discussed below, where a cutoff of 60 Ry was used. Exchange and correlation were treated in the local density approximation (LDA), with generalized-gradient-approximation corrections to the LDA shown to be small for Mo.

We now turn to the simulation of the high-pressure melt curve in Mo as a benchmark test of the  $T_{el}$ -dependent MGPT potentials. Our central MD/MGPT and QMD results are displayed in Fig. 4 together with previous fitted QMD melt calculations [9] and experimental melt data obtained from isobaric [18] and shock [19] measurements. All of the present melt results have been obtained with the standard two-phase simulation method, in which equilibrated solid (bcc) and liquid sub-cells are placed in contact and

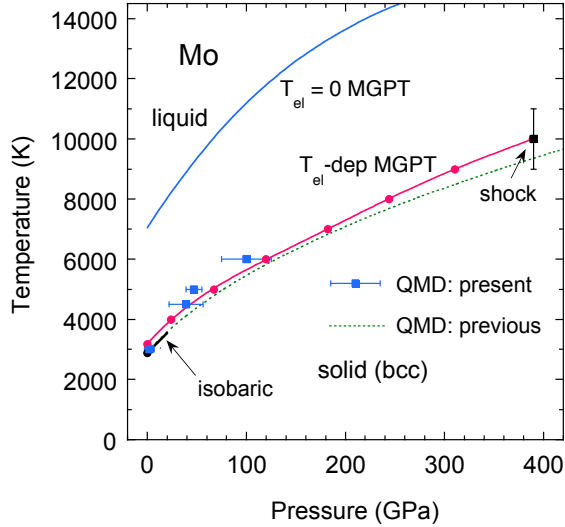


**Fig. 4** High-pressure melt curve for Mo, as obtained from MD simulations with  $T_{el} = 0$  and  $T_{el}$ -dependent MGPT potentials and from the present and previous (Ref. 9) QMD simulations, and as compared to experimental isobaric (Ref. 18) and shock (Ref. 19) data.

the motion of the solid-liquid interface monitored as a function of temperature. The full 256-atom (128 solid plus 128 liquid) computational cell used in our two-phase QMD melt simulations represented the maximum number of atoms that we could reasonably treat for Mo. Each calculated melt point required 7-10 two-phase simulations, with a time step of 1.2 fs and a simulation time of  $\sim 1$  ps. A total of four QMD melt points up to 100 GPa were so obtained. In contrast, cell size was not a limitation in the MD/MGPT melt simulations, and the  $T_{el}$ -dependent MGPT melt curve was obtained with 87,808-atom simulations to produce minimal statistical scatter in the eight calculated points up to 400 GPa. We have also confirmed the weak-coupling result of Ref. 14 in the  $A_{el} = 0$  limit of Eq. (1) by simulating the Mo melt curve with the best available  $T_{el} = 0$  MGPT potentials based on canonical  $d$  bands [17], showing clearly the factor of two overestimate of melt temperatures. The introduction of non-canonical  $d$  bands lowers this result, but only when electron temperature is included through the  $T_{el}$ -dependent MGPT potentials is the calculated melt curve brought into close proximity of the QMD and experimental data, yielding good agreement among these results. These latter results also agree with the additional DFT simulation of the Mo melt curve by Cazorla *et al.* [7].

DFT-based melt calculations in bcc Mo and Ta, including both the present results and previous calculations [6-9,11], have all produced steep  $T$ - $P$  melt curves with increasing pressure, in general agreement with *dynamic* experimental data, but in sharp contrast to the nearly flat  $T$ - $P$  melt curves obtained in previous *static* diamond-anvil-cell (DAC) measurements [1,3]. This has led to a decade of controversy concerning the correct interpretation of the DAC measurements, including theoretical evidence of possible solid-solid phase transitions prior to melt [6,9-11] and a recent DAC measurement of a steep  $T$ - $P$  melt curve in Ta [4]. Particularly interesting in this regard is the possibility of a rich polymorphism in the high  $T$ - $P$  solid beneath the melt curve in such materials. Using small-cell ( $\leq 128$  atoms) QMD simulations, Belonoshko *et al.* [9] have found that the fcc structure in Mo melts at a higher temperature than bcc above  $\sim 150$  GPa, which implies that the fcc phase is thermodynamically more stable than bcc in that regime. To explore this issue further, we have made an initial study of high  $T$ - $P$  polymorphism in Mo using our  $T_{\text{el}}$ -dependent MGPT potentials. We focused on a single volume corresponding to  $P \sim 65$  GPa at 5000 K near melt, and considered five candidate structures: bcc, fcc, fct (face-centered tetragonal,  $c/a = 1.107$ ), hcp ( $c/a = 1.633$ ) and hex- $\omega$  (hexagonal omega,  $c/a = 0.56$ ). Unlike bcc, the fcc, fct, hcp and hex- $\omega$  structures are all mechanically unstable at  $T = 0$  for this volume, with calculated imaginary phonon frequencies. Using MD/MGPT simulations with up to 2048 atoms, we have determined that each of the non-bcc structures is mechanically stabilized at 5000 K. This stability is driven by large anharmonic vibrational effects, which are enhanced by  $T_{\text{el}}$  and estimated by  $Q_{\text{ah}} = 100(1 - E_{\text{th}} / 3k_{\text{B}}T)$ , where  $E_{\text{th}} = \langle F_{\text{el}} \rangle - E_0$ . Here  $Q_{\text{ah}} = 7.4\%$  in bcc Mo at 5000 K, whereas  $Q_{\text{ah}}$  is 3-6 times larger in the other phases: 28.9% in fcc, 25.4% in fct, 20.8% in hcp and 43.3% in hex- $\omega$ . Once equilibrated at 5000 K, we raised the temperature slowly in each of the five structures until melt was observed, establishing a constant-volume critical melt point  $T_c$  for each phase. We then used the  $Z$ -method of Belonoshko *et al.* [9] to estimate the thermodynamic melt temperature  $T_m < T_c$ . While  $T_m$  was not well established for the hcp structure by this procedure, it was for the other four candidate structures, with the final result  $T_m^{\text{fcc}} > T_m^{\text{fct}} > T_m^{\text{bcc}} > T_m^{\text{hex-}\omega}$ . Thus both the

fcc and fct structures were found to be more stable than bcc under the assumed conditions. This supports the hypothesis that multiple solid phases, either stable or metastable, could be present in Mo under high  $T$ - $P$  conditions.

This work was performed under the auspices of the U. S. Department of Energy by Lawrence Livermore National Laboratory under contract No. DE-AC52-07NA27344, with financial support from DOE SciDAC grant ER25788 and computing support from the LLNL Institutional Computing Grand Challenge program.

## References

- [1] D Errandonea *et al.*, Phys. Rev. B **63**, 132104 (2001) and J. Phys. Condens. Matter **15**, 7635 (2003).
- [2] J. H. Nguyen and N. C. Holmes, Nature **427**, 339 (2004).
- [3] D. Santamaria-Perez *et al.*, J. Chem. Phys. **130**, 124509 (2009).
- [4] A. Dewaele *et al.*, Phys. Rev. Lett. **104**, 255701 (2010).
- [5] D. Alfè, M. J. Gillan and D. G. Price, Nature **401**, 462 (1999) and A. Laio *et al.*, Science **287**, 1027 (2000).
- [6] J. A. Moriarty *et al.*, J. Phys: Condensed Matter **14**, 2825 (2002).
- [7] C. Cazorla *et al.*, J. Chem. Phys. **126**, 194502 (2007).
- [8] S. Taioli *et al.*, Phys. Rev. B **75**, 214103 (2007).
- [9] A. B. Belonoshko *et al.*, Phys. Rev. Lett. **100**, 135701 (2008).
- [10] C. J. Wu *et al.*, Nature Mater. **8**, 223 (2009)
- [11] L. Burakovsky *et al.*, Phys. Rev. Lett. **104**, 255702 (2010).
- [12] N. D. Mermin, Phys. Rev. **137**, A1441 (1965).
- [13] R. Q. Hood, L. H. Yang and J. A. Moriarty, Phys. Rev. B **78**, 24116 (2008).
- [14] J. A. Moriarty, Phys. Rev B **49**, 12431(1994) and **42**, 1609 (1990).
- [15] J. A. Moriarty, Phys. Rev. B **38**, 3199 (1988).
- [16] V. Recoules *et al.*, Phys. Rev. Lett. **96**, 055503 (2006).
- [17] J. A. Moriarty *et al.*, J. Mater. Research **21**, 563 (2006).
- [18] J. W. Shaner, G. R. Gathers and C. Minichino, High Temp. High Pressures **9**, 331 (1977).
- [19] R. S. Hixson *et al.*, Phys. Rev. Lett. **62**, 637 (1989).